ARTICLE OPEN

Check for updates

An assessment of the ENSO-monsoon teleconnection in a warming climate

Bidyut Bikash Goswami [1] and Soon-Il An [2,3,4 ✉]

The El Niño-Southern Oscillation (ENSO) and the Indian summer monsoon (ISM, or monsoon) are two giants of tropical climate. Here we assess the future evolution of the ENSO-monsoon teleconnection in climate simulations with idealized forcing of CO_2 increment at a rate of 1% year^{-1} starting from a present-day condition (367 p.p.m.) until quadrupling. We find a monotonous weakening of the ENSO-monsoon teleconnection with the increase in CO_2. Increased co-occurrences of El Niño and positive Indian Ocean Dipoles (pIODs) in a warmer climate weaken the teleconnection. Co-occurrences of El Niño and pIOD are attributable to mean sea surface temperature (SST) warming that resembles a pIOD-type warming pattern in the Indian Ocean and an El Niño-type warming in the Pacific. Since ENSO is a critical precursor of the strength of the Indian monsoon, a weakening of this relation may mean a less predictable Indian monsoon in a warmer climate.

INTRODUCTION

The Indian summer monsoon (ISM, or simply, monsoon) rainfall (ISMR) is the backbone of the socio-economic well-being of the people in India. Especially the farmers of the rain-fed farmlands in India heavily rely on the summer monsoon rainfall. Despite the remarkable recurrence of the ISM rainfall every year, considerable year-to-year variability makes its prediction a challenging issue[1]. Major sources of its predictability come from the slowly varying boundary conditions[2]. The equatorial Pacific sea surface temperature (SST) anomalies associated with the El Niño-Southern Oscillation (ENSO) are one such source[3].

Often, the cold phase of the ENSO or La Niña is associated with a strong ISM and the warm phase of the ENSO or El Niño is associated with a weaker ISM[4]. However, following an above-normal monsoon rainfall in the year 1997 despite a strong El Niño event, Kumar et al.[5] suggested that the ENSO-monsoon relationship might have broken down post-1980 due to global warming. However, the deficit ISMR in 2002 and 2004 (that were El Niño years) motivated Annamalai et al.[6] to investigate the evolution of the ENSO-monsoon teleconnection under global warming using climate model simulations. Comparing historical simulations and global warming runs, Annamalai et al.[6] concluded that the ENSO-monsoon relation may remain intact under global warming. In substance, there is no clear consensus on whether the ENSO-monsoon relationship will weaken or stay intact amidst a warming climate[7,8]. While some studies find that the ENSO-monsoon relationship will stay stable under global warming[6,9,10]; some find that it is going to weaken[11] and some argue that it is going to be a battle between circulation changes and moisture availability[12]. A recent study by Bódai et al.[13] even reported an increase in the strength of this teleconnection albeit with some cautionary notes on the choice of indices and methodology to evaluate the teleconnection.

A crucial aspect of the ENSO-monsoon teleconnection is the role of the Indian Ocean Dipole (IOD)[14,15] in it. The importance of the IOD is evident from the fact that about 50% of the positive IODs (pIODs) occur when the Pacific ocean exhibits an El Niño like state[16,17]. Several studies that investigated the variability and diversity of the ENSO-monsoon teleconnection find that the IOD plays a critical role in modulating the ENSO-monsoon relation[18,19]. Ashok et al.[18] found that the co-occurrence of El Niño and pIOD reduces the impact of El Niño on the monsoon. While El Niño drives large-scale subsidence over the monsoon domain, pIOD makes more moisture available to the monsoon winds reducing the negative impact of El Niño on the monsoon rainfall. In fact, regarding the changing ENSO-monsoon relation, few studies have reported changes in the co-occurrence of IOD events with ENSO[20–22]. Analyzing the Climate Model Intercomparison Project (CMIP) model simulations under warming scenarios some recent studies argue that extreme-positive IODs may increase in the future[23–25].

The climate models are the only tools to investigate the future evolution of the ENSO-monsoon relation. Despite limitations in our understanding of the processes that connect the ENSO, monsoon, and IOD, and the systematic biases in the climate models in mimicking these processes, the climate models perform reasonably well in capturing major features of these climate phenomena and their associations[26,27]. As per the latest Intergovernmental Panel on Climate Change (IPCC) Sixth Assessment Report (AR6), for higher emissions, many models suggest an El Niño-like warming of the mean state in the Pacific Ocean[28–30]. This is intriguing because El Niño-like warming can potentially prohibit the increase in seasonal mean ISM rainfall[31–34]. However, the same IPCC AR6 reports that the ISM rainfall is projected to increase during the 21st century in response to continued global warming[35–39]. On the other hand, the report also indicates pIOD-like warming of the mean state in the Indian Ocean[23,40], which can be expected to enhance ISM seasonal mean rainfall. These projections of the ISM, ENSO, and IOD in the IPCC AR6 suggest that the IOD may play a crucial role in the future evolution of the ENSO-monsoon teleconnection.

Unfortunately, realistic simulation of the ENSO-Monsoon teleconnection even in a historical run is still a struggle for many state-of-the-art climate models[26]. Modulation of the strength of

[1]Institute of Science and Technology Austria (ISTA), Klosterneuburg, Austria. [2]Irreversible Climate Change Research Center (IRCC), Yonsei University, Seoul, South Korea. [3]Department of Atmospheric Sciences, Yonsei University, Seoul, South Korea. [4]Pohang University of Science and Technology, Pohang, South Korea. ✉email: sian@yonsei.ac.kr
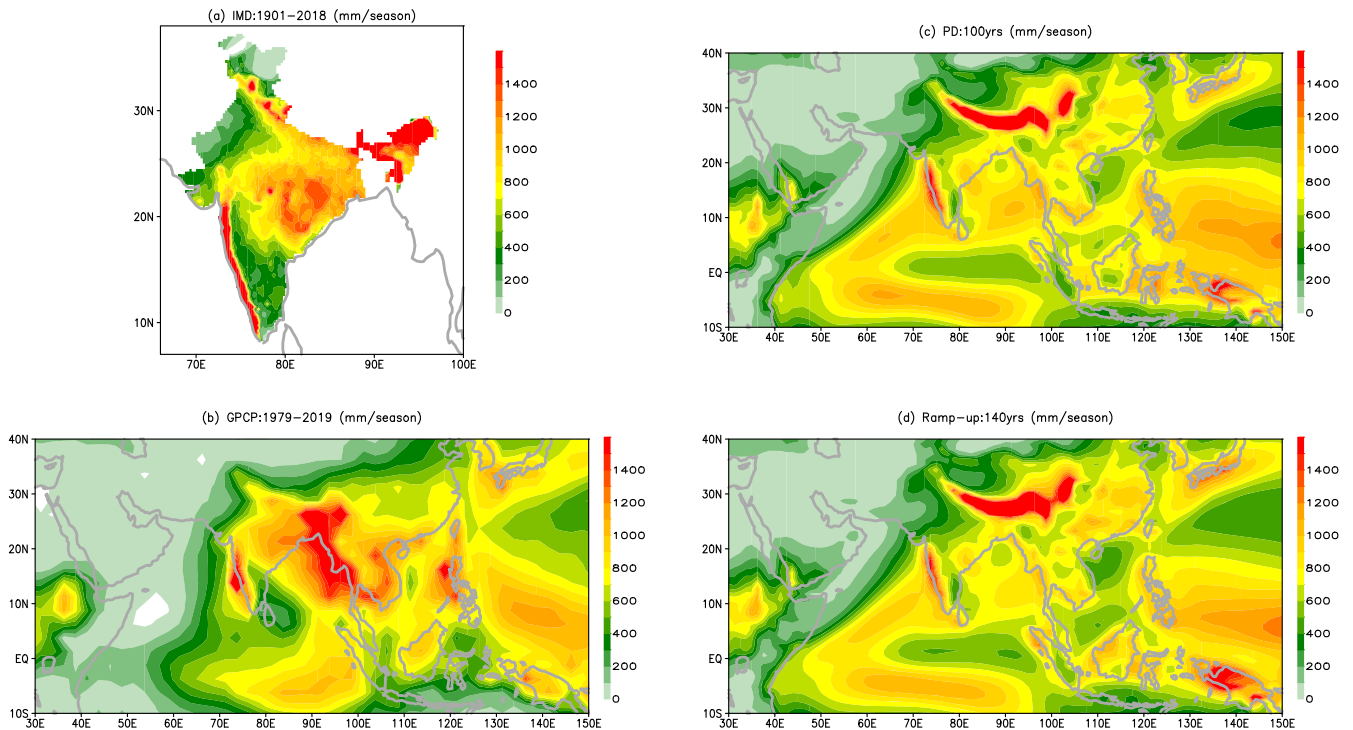
Fig. 1 **The observed and simulated Indian summer monsoon rainfall.** JJAS mean rainfall (**a**) IMD data (1901-2019); (**b**) GPCP (1979-2019); (**c**) PD simulation (last 100 years of simulations); (**d**) RU simulation (140 years).

this teleconnection over time, for example, decadal time scales[41–43], makes it very harder for the models to simulate this relationship. Intermodel diversity in the simulation of monsoon and ENSO leads to large uncertainty in the projection of ENSO-monsoon relation[8]. While it is desirable to obtain a multimodel agreement on the future projection of ENSO-monsoon relation, given the large intermodel diversity, investigations based on the simulations by a single model can also be insightful and instructive. A plausible option is to analyze ensemble simulations[13]. Idealization of the forcing field is also helpful in understanding the evolution of the ENSO-monsoon teleconnection under global warming[6,9].

With this background, we analyzed the relationship between monsoon and ENSO in an idealized simulation with monotonically increasing CO_2 forcing. This monotonic increase of CO_2 or ramp-up phase is part of a transient CO_2 reversibility experiment with CESM1.2 (e.g., An et al.[44]). In this reversibility experiment, CO_2 forcing is gradually increased from a present-day value of 367ppm at a rate of 1% year^{-1} for 140 years until quadrupled (ramp-up (RU)) and then decreased at the same rate for the next 140 years (ramp-down (RD)). Before the ramp-up period, a constant CO_2 scenario was conducted for 900 years, with 367ppm as the present-day (PD) climate simulation. The basic experimental design is the same as the CO_2 removal Model Intercomparison Project (CDRMIP) simulations, except staring from the present-day level of CO_2 concentration rather than preindustrial level[45]. The model experiment details are provided in the Methods section.

RESULTS
Mean State
The climate model that we have used, CESM, is one of the participating models in the CMIP. It is a state-of-the-art climate model. CESM1 is fairly good at simulating ENSO[46] and ISM[47]. The model also simulates the ENSO-monsoon connection fairly well[47]. Since the CESM1 model has been well studied for its ability to simulate ENSO, monsoon, and their teleconnection[47] we have

refrained from showing a detailed analysis of the same in this study. Nonetheless, the June-July-Aug-Sept (JJAS) daily mean rainfall climatology simulated in the PD simulation and in the ensemble mean of the RU period (which is the main focus period of this study) is shown in Fig. 1. The model simulates the ISM rainfall climatology reasonably well in the PD simulation and the RU ensemble mean. The mean monsoon simulations exhibit biases that are chronic to many state-of-the-art climate models[48–50]. Against the backdrop of these biases, our PD simulation of mean monsoon rainfall climatology (Fig. 1c) is fairly realistic and is at par with the best climate models. In the RU simulations (Fig. 1d), the major features of the monsoon rainfall distribution and strength are retained and do not show any dramatic changes.

Simulation of the ENSO-Monsoon correlation in RU simulation
A simple way to assess the ENSO-monsoon teleconnection is to calculate the simultaneous correlation between monsoon rainfall over India and SST. Figure 2 depicts these correlations for observations, PD simulation, and RU (mean of 28 ensembles) simulations. In the PD simulations, the model could capture the overall correlation patterns in the Indian and Pacific Oceans but performs poorly in the Atlantic. On a close look, several shortcomings are evident in the PD simulation. For example, in the Indian Ocean, overly strong correlation values are almost everywhere, with opposite correlations in the northern Bay of Bengal region. In the Pacific Ocean, the correlation over the eastern Pacific is in streaks of high and low values diverging from the central Pacific and negative correlation values continue too far west (touches Borneo). Meehl et al.[51] found similar biases in the ENSO-monsoon association in CCSM4, which is a subset of CESM1 that we have used. They argued that a shift in the simulation of the Walker cell and model internal variability in the monsoon region may be responsible for this bias in the correlation field. A faithful simulation of the Walker cell is critical to simulate the ENSO-monsoon teleconnection[6,52]. ENSO influences the Indian monsoon through interactions between the equatorial Walker
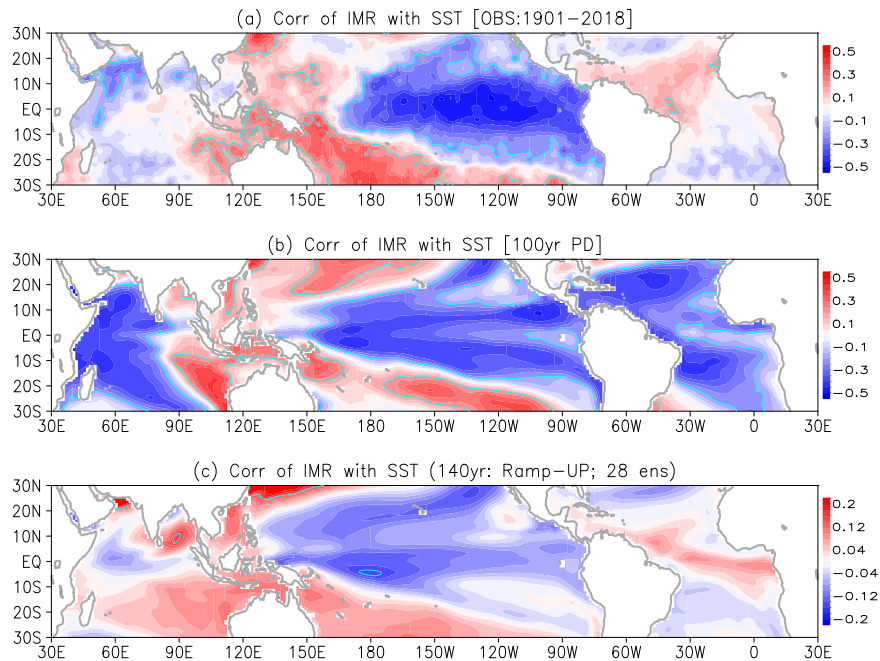
Fig. 2 Correlation of the Indian summer monsoon rainfall with tropical sea surface temperatures. One-point correlation of JJAS mean rainfall over CI region (CI: 18°N-28°N and 65°E-88°E, as defined by Rajeevan et al.[87]) with JJAS mean SST anomalies for (**a**) observations (rainfall from IMD and SST from HadISST data); (**b**) PD simulation (last 100 years of simulations); (**c**) RU simulation (140 years). Correlation values above 90% significance level are indicated by the cyan colored contour.

circulation and the regional monsoon Hadley circulation. The model could simulate monsoon Hadley and Walker cells reasonably well in the PD simulations (Supplementary Figure S1). We note that the Walker cell weakened in the RU simulations compared to the PD period. Since our goal in this study is to gain insight into the evolution of the ENSO-monsoon relation in a warming scenario, keeping the biases in the PD simulation in the background we now focus on the RU simulations. Since the RU simulation analysis is based on 28 ensemble runs, the results can be insightful despite the biases in the PD simulation. In the RU simulations, the most striking feature is the overall weakening of the correlation value over the Indian and the Pacific Oceans with the major correlation pattern remaining intact, except over the south-western IO. The decrease in correlation value over the Pacific essentially indicates a weakening of the ENSO-Monsoon teleconnection. This raises a natural follow-up question: what is the nature of this decrease? To address this question, we analyzed the time evolution of strength of the correlation between ENSO and monsoon rainfall.

Figure 3 depicts the 21-year running correlation between NINO3.4 and ISMR in the RU simulations. For a 21-year running window, a correlation value of -0.37 is 90% significant. The ENSO-monsoon correlation during the RU simulation is not statistically significant. However, it should be noted that 25% of the ensembles exhibit significant negative correlation in the first 21-year window. The slope of weakening of correlation is statistically significant at 90%. Bódai et al.[13] argued that the temporal correlation metric may not provide the correct information about the ENSO-monsoon relation in a changing climate. However, since these correlations area-averaged for 28 different ensembles they are reliable. Multi-decadal variability is evident from the changes in the strength of correlation. Multi-decadal variability in ENSO-monsoon teleconnection has been reported by several earlier studies using observation data[5,41,53,54]. It is beyond the scope and focus of our analysis to investigate how much of this multi-decadal variability is due to internal variability[51,55] and if any part is attributable to external forcing. We note in Fig. 3 that on top of this multi-decadal variability, the strength of the correlation

gradually weakens as the CO_2 forcing increases. Under transient greenhouse gas forcing, Ashrit et al.[55] did not find any remarkable weakening of the ENSO-monsoon relation. Their analysis, however, was based on one transient simulation. The risk of using only one simulation is evident from the diverse results reported by Ashrit et al.[55–57]. In our analysis, all 28 ensembles indicate a weakening of the ENSO-monsoon teleconnection.

Cause of ENSO-Monsoon teleconnection weakening

Analyzing the weakening in the observed ENSO-monsoon teleconnection post-1980, Kumar et al.[5] suggested a southeastward shift of the subsiding branch of the Walker circulation from over the Indian monsoon domain to over the Maritime continents to be a possible reason. This suggestion of Kumar et al.[5] stemmed from their comparative analysis of the El Niño composite of the 200hPa velocity potential (VP) for pre and post-1980. The VP (either at upper levels, viz, 200hPa, or at lower levels, viz, 850hPa) has been a widely used metric since the work of Kumar et al.[5] in studies that investigated the changes or diversity in the ENSO-monsoon teleconnection[17–19,56–62]. El Niño composites of VP indicate a weakening of subsidence over the Indian monsoon domain during RU period consistent with a weaker Walker circulation during RU period (Supplementary Figure S2). Since our model simulations suggest a monotonous weakening of the ENSO-monsoon teleconnection in the 140 years of the RU simulations (Fig. 3), we also performed an analysis by comparing the El Niño composite of 200hPa and 850hPa VP for the first and last 70 years of the RU simulation (averaged over all the 28 ensembles) (Supplementary Figure S2). There is a strengthening of Walker circulation during the 2nd half of the RU period. However, we did not find these differences statistically significant. To further investigate we also contrasted the El Niño composites of equatorial Walker circulation and the regional monsoon Hadley circulations for the first and last 70 years of the RU simulation (Supplementary Figure S3) and we did not find the differences significant. Sabeerali et al.[63] reported a significant increase in the association of the monsoon rainfall with Atlantic zonal mode
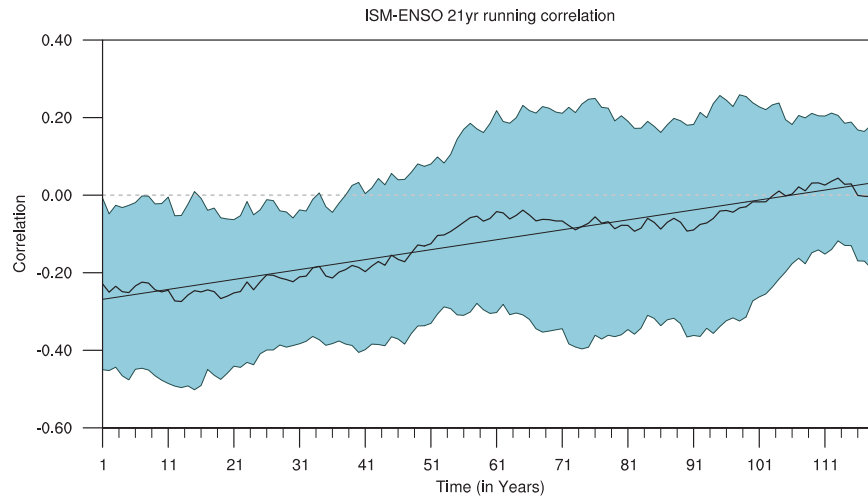
Fig. 3 Time-evolution of ENSO-Monsoon teleconnection strength. JJAS mean NINO3.4 (SST anomalies averaged over 5°S–5°N, 120°–170°W) and ISMR (over CI) 21-year running correlation. The blue color depicts spread of ensembles (one standard deviation).
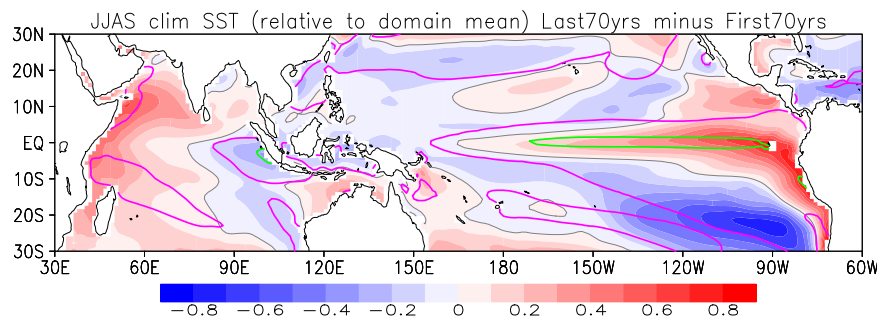

Fig. 4 Comparision of the boreal summer mean SST over the Indian and Pacific basins between the two halves of the ramp-up simulation. Climatological JJAS mean sea surface temperature difference between the first 70 years and the last 70 years of the ramp-up period. Domain mean SST is subtracted from the depicted field. The magenta and lime contours indicate 90% and 99% significant contour values.

(AZM)[64] a.k.a, the Atlantic Niño[65] as the ENSO-monsoon tele-connection weakens. We repeated the correlation analysis (as in Fig. 3) to investigate any significant change in the ISMR association with the AZM. We found the correlations were weak (hovering around 0 value) for the whole 140 years of the RU simulation (Supplementary Figure S4). The correlation values, however, changed signs from negative to positive and exhibited multi-decadal modulations in their strength. A one-point correlation of the monsoon rainfall with SST (after removing the ENSO signal following Pottapinjara et al.[66]) is shown in Supplementary Figure S5. The model did not capture the correlation pattern accurately over the tropical Atlantic. However, Atlantic SST and Indian monsoon connection have been reported to have changed over time[63]. Using observation data and model experiments, Pottapinjara et al.[66–68] advocated for a thermodynamic mechanism involving oceanic heat content to explain Atlantic zonal mode and Indian monsoon teleconnection. The model's fidelity in simulating the tropical Atlantic Ocean and Indian monsoon teleconnection requires further analysis, which is beyond the scope of the current study. Coming back to the speculation of a southeastward shift of the Walker circulation over the western Pacific by Kumar et al.[5], the postulated dynamical reason behind Kumar et al.[5]'s speculation was the expansion of the Indo-Pacific warm pool recently documented by Roxy et al.[69]. Therefore, to investigate further the reasons behind the weakening ENSO-monsoon teleconnection in our simulations, we analyzed the SST warming. We contrasted the warming between the first and last 70 years of the RU simulation. Figure 4 depicts the ensemble mean

JJAS mean SST for the first 70 years subtracted from that for the last 70 years. Essentially this represents the JJAS warming pattern in the RU simulation. To bring out the warming pattern clearly, the domain-mean value of the warming over each ocean basin is subtracted from each grid and what emerges is an El Niño-type warming pattern in the Pacific and a pIOD-type warming pattern in the Indian Ocean. This warming pattern of the Indian Ocean is consistent with earlier studies which find that the western and northern regions of the Indian Ocean are projected to warm faster than the eastern and southern parts[23–25,70]. It suggests more pIODs in a warmer climate. On the other hand, more El Niños can be expected based on an El Niño-like warming pattern in the Pacific in a warmer climate[71]. Considering both El Niño and pIODs may occur more often, a warmer climate may exhibit co-occurrences of El Niños and pIOD more often. Ashok et al.[18] showed that when El Niño and pIOD co-occur, ISMR encounters competing impacts from El Niño and pIOD. Ratna et al.[72] also found contrasting impacts from the Indian Ocean and the Pacific owing to a pIOD and El Niño-like SST anomalies in the Pacific in the year 2019. Therefore, more El Niño and pIOD co-occurrence may result in a decreased influence of El Niño (as well as of IOD) on the ISMR. To assess any change in the co-occurrences of pIOD and El Niño with warming in the RU simulations we analyzed the joint probability distribution function (PDF) of DMI (IOD index, see method) and NINO3.4. Figure 5 depicts the NINO3.4-DMI bivariate PDF averaged for all 28 ensembles for the first and the last 70 years. The joint PDF for the first 70 years is consistent with the observed NINO3.4-DMI association (Stuecker et al.[73], see Fig. 2a).
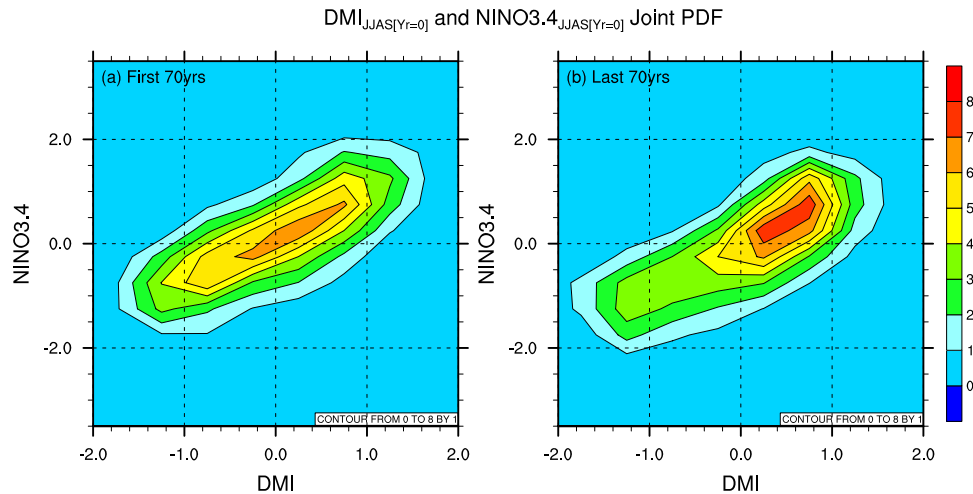
DMI$_{JJAS[Yr=0]}$ and NINO3.4$_{JJAS[Yr=0]}$ Joint PDF

Fig. 5 Joint PDF of ENSO and IOD during the two halves of the ramp-up simulation. Bivariate PDF of JJAS mean DMI and NINO3.4 (**a**) first 70 years, (**b**) last 70 years, of RU simulation.
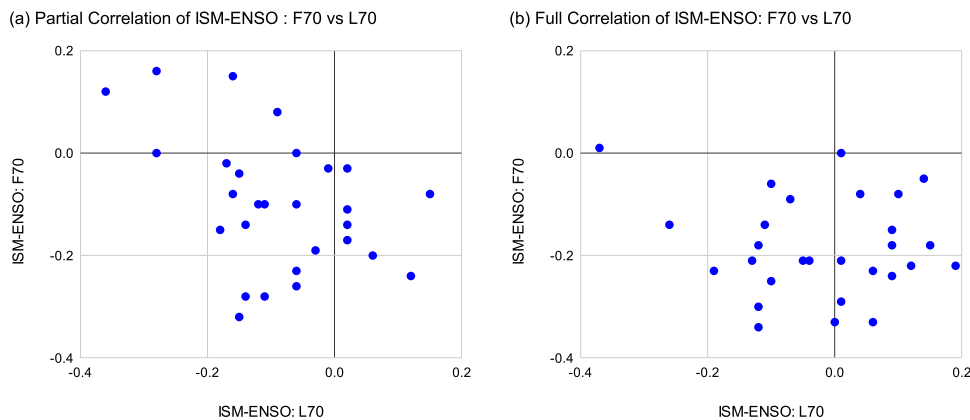

Fig. 6 ENSO-monsoon partial and Pearson correlations. Scatter of ENSO-monsoon partial correlations in 28-ensembles between first and last 70 years of the RU simulations are depicted in panel (**a**); and the same for Pearson correlations is depicted in panel (**b**).

However, during the last 70 years, the distribution is more heavily skewed towards more El Niño and pIOD co-occurrences.

Examining velocity potential (Supplementary Figure S2) we did not see any remarkable changes in the Walker circulation that, following the argument of Kumar et al.[54], can explain the weakening of the ENSO-monsoon correlation in our simulations. If anything, we noticed a strengthening of the Walker circulation in the last 70 years of the RU simulations compared to the first 70 years. Strengthening of the Walker circulation is not surprising because mean tropical Pacific SST increases with increasing CO_2, which leads to strong convection over warmer SST anomalies. Following this discrepancy, we looked at the the change in SST warming pattern (Fig. 4) and the joint PDF of NINO3.4 and DMI indices (Fig. 5). To elicit further the possible role of the IOD state in the ENSO-monsoon teleconnection we performed a partial correlation analysis (Fig. 6, and also supplementary Figure S6). Figure 6a depicts that ENSO-monsoon partial correlation does not show a remarkable change in the sense that, the majority of the ensemble members exhibit a negative correlation in both halves of the RU simulation. However, the Pearson (or full) correlation values (Fig. 6b) between ENSO-monsoon show strong diversity in the last 70 years (having both positive and negative values) and a weaker absolute value of the correlations. This indicates that the ENSO-monsoon correlation if we ignore the IOD influence, does not change dramatically. It does, however, change when we do include the impact of the IOD on the monsoon. Although this analysis, depicted in Fig. 6, does not underpin any particular phase

of IOD that is responsible for contaminating the ENSO-monsoon correlations, it is consistent with our finding of more frequent El Nino-pIOD co-occurrences during the second half (last 70 years) of the RU simulations.

El Niño and pIOD co-occurrences

In this section, we explore the reason behind increasing El Niño and pIOD co-occurrences as the climate warms under increasing CO_2 forcing. Co-occurrences of El Niño and pIOD are quite common in observations. About 50% of El Niños occur with pIOD in the Indian Ocean[16,17]. Both ENSO and IOD are extremely well-coupled phenomena, and they are associated in multiple ways[74]. But the nature of their association is not clear. Some studies found a profound consequence of IOD on the following year's ENSO[75,76] and some argue ENSO can initiate many IOD events[77,78]. On the other hand, some studies question the existence of IOD as an independent mode[73,79]. This debate will need further research to settle. Nonetheless, to understand the cause behind more pIODs in our simulations we compared the distribution of DMI values with and without the influence of ENSO in the first and last 70 years of the RU simulations (Fig. 7). We find that more pIODs occur in the last 70 years (Fig. 7a), consistent with the joint PDF (Fig. 5). However, when the ENSO signal is removed, the DMI distributions for the first and last 70 years are fairly similar and not skewed (Fig. 7b). What makes an El Niño drive a pIOD more often as the climate warms in our simulations is yet to be investigated.
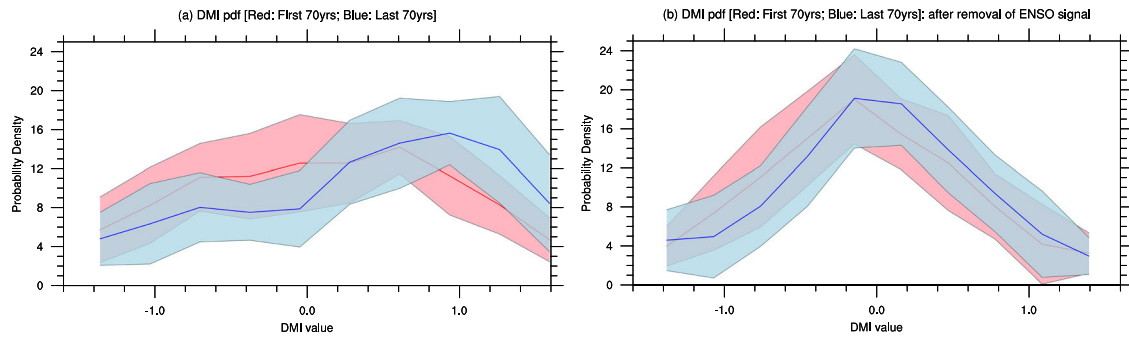
Fig. 7   Comparision of IOD distributions between the two halves of the ramp-up simulation associated with and without El Nino influence. a PDF of DMI for first 70 years (in red) and last 70 years (in blue). **b** Right hand side panel PDFs are computed after removal of the ENSO signal.
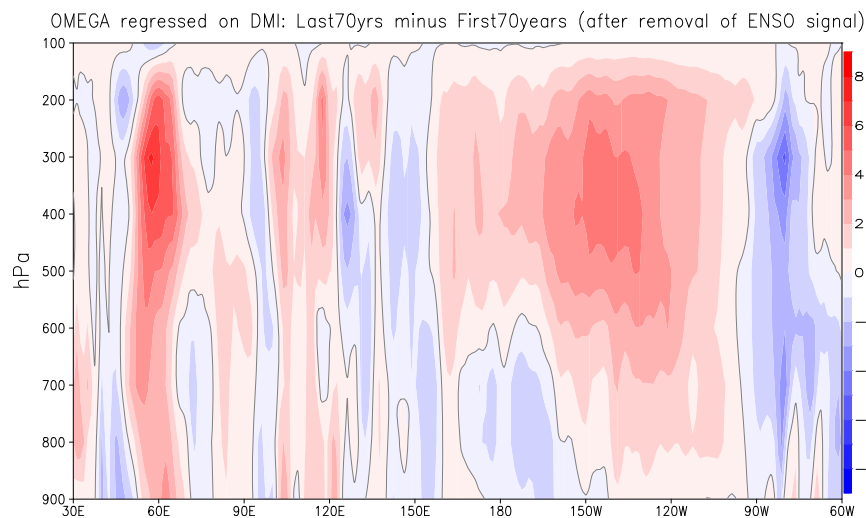

Fig. 8   Comparison of zonal circulation over the tropics between the two halves of the ramp-up simulation associated with IOD (excluding El Nino influence). Longitude-height cross-section of the JJAS mean pressure vertical velocity (Omega, Pa/Sec x 1000) regressed onto the Dipole Mode Index (DMI) (ENSO signal removed from both Omega and DMI), and then averaged over 5°S-5°N for the first 70 years subtracted from the same for the last 70 years of the RU simulation.

Nonetheless, the analyses presented in Fig. 7 suggest that as the climate warms with a pIOD-like warming pattern in the IO and an El Niño-like warming pattern in the Pacific, pIODs will occur more often as a response to El Niño. Following up this analysis, we compared the Walker cell circulations for the pIOD events (ENSO signal removed) contrasting the first and last 70 years of RU simulations. We found anomalous sinking motion over the eastern Pacific (Fig. 8) suggesting a stronger tendency of the pIODs to weaken El Niño during the last 70 years. This motivated us to check the NINO3.4 value of the following-year winter to examine if a La Niña follows. We repeated the joint PDF analysis for DMI and NINO3.4 as depicted in Fig. 5, except we considered the DMI value during Sep-Oct-Nov and the NINO3.4 value during the following-year winter (that is, Dec-Jan-Feb 12 months post the DMI value). The lagged NINO3.4-DMI joint PDF depicted in Fig. 9 suggests a more frequent transition from El Niño to La Niña in the last 70 years of the RU simulations. Jointly Figs. 5, 7, and 9 suggest more frequent occurrences of an El Niño driving a pIOD and the pIOD, in turn, causing the El Niño to transition to La Niña in a warmer climate. These results indicate a stronger association between IOD and ENSO in a warmer climate.

Detailed explanations for a stronger IOD-ENSO association in the last 70 years of the RU simulations will be investigated in a future study. Nonetheless, since we find a stronger association between IOD and ENSO and a weaker ENSO-monsoon correlation in the last 70 years of the RU simulations, we examined if the

ENSO-monsoon correlation can be expressed as a linear function of the ENSO-IOD correlation. We found that (figure not shown) the correlations are not consistent with what we observed in our earlier analysis. One possible explanation can be because the correlation metric depends on both positive and negative values of IOD and ENSO indices, perhaps the negative values of the indices are not as well correlated as the positive values. In observations also, more instances of co-occurrence of El Niño and pIODs are seen than La Niña and negative IODs[16,17]. Moreover, the response of the Indian monsoon may not be symmetric to the different phases of ENSO[80]. Intriguingly, when we arranged the change in the ENSO-monsoon correlation in the last 70 years of the RU simulations compared to the first 70 years according to the DMI trend for the different ensembles (figure not shown), a positive DMI trend (increasing east-west SST contrast in the equatorial Indian Ocean) is found to be related to a weaker ENSO-monsoon relationship albeit without much statistical confidence. Detailed analysis will be required for a better understanding of the ENSO-IOD association in our model-simulated climate. For now, what we do know with confidence is that pIODs are associated with the weakening of the ENSO-monsoon correlation in a warmer climate in the RU simulations.

The weakening ISM-IOD relation in a warmer climate in our model results would be a consequence of a competing effect of pIOD and El Niño on the ISMR (Supplementary Figure S7). Therefore, an increase in pIOD does not necessarily indicate a
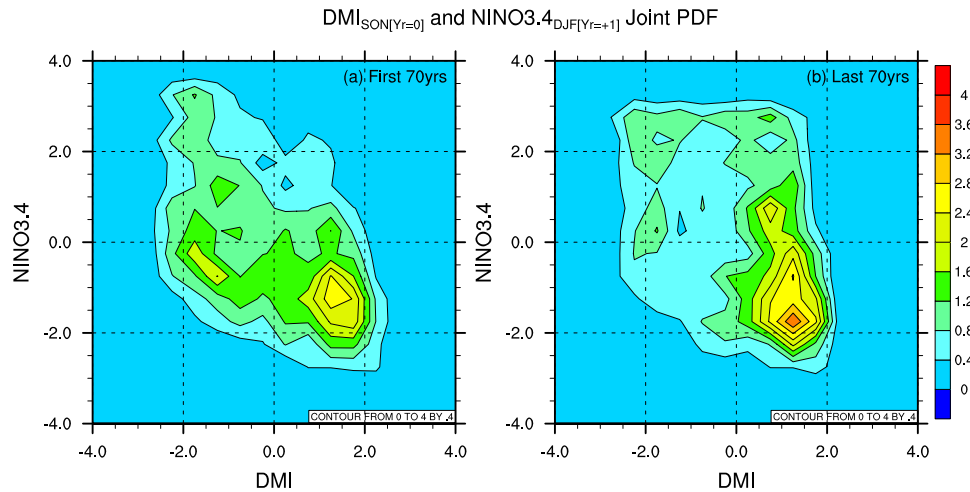
DMI$_{SON[Yr=0]}$ and NINO3.4$_{DJF[Yr=+1]}$ Joint PDF

Fig. 9 Lagged joint PDF of ENSO and IOD (IOD leading ENSO by a year) during the two halves of the ramp-up simulation. Bivariate PDF of SON mean DMI (year=0) and DJF mean NINO3.4 (year=1) (**a**) first 70 years, (**b**) last 70 years, of RU simulation.

stronger monsoon-IOD relation since these pIODs are posited to co-occur with El Niño. Noteworthy, since we do see more occurrences of pIOD during the last 70 years and since pIODs are favorable for ISM rain, we find that the nature of the correlation between DMI and ISM gradually transitions from negative to positive values during the RU simulation. Given the weakening influence of both ENSO and IOD on ISM rainfall and no remarkable strengthening of the ISMR association with the Atlantic zonal mode (Supplementary Figure S4), our simulations suggest that ISMR prediction may become more challenging in a warming climate. In this regard, partial correlations are useful to isolate interrelations between three variables, for example, ENSO, monsoon, and IOD. During the first half (1st -70th year) of the increased CO_2 forcing, both Pearson and partial correlation of ENSO with monsoon are negative, for a majority of the ensemble members. However, during the second half (71st-140th year), while their partial correlations are negative in general, the Pearson correlations are indecisive and generally weaker in strength. Similar changes in monsoon-IOD correlations are also noted (except that, partial monsoon-IOD correlations are positive, as expected). These changes in correlations need detailed examinations. Nonetheless, ENSO-monsoon and monsoon-IOD relations compete against each other more during the second half of the simulations.

DISCUSSION

In this study, we examined ENSO-monsoon teleconnection in 28 ensembles of idealized climate simulations that mimic climate warming via linearly increasing CO_2 concentration at a rate of 1% year^{-1} from 367 ppm until quadrupling. We used CESM1.2 to perform these simulations. All the ensembles agree that the teleconnection would weaken in a warmer climate while its strength would continue to exhibit multi-decadal variability. Further investigation revealed that an increasing number of co-occurrences of El Niño and pIOD in a warmer climate causes this weakening. We found that during El Niño the Indian Ocean responds with a pIOD more often in a warmer climate. Furthermore, the co-occurrences of El Niño and pIOD are attributable to mean state warming of the SST, which resembles a pIOD-type warming pattern in the Indian Ocean and an El Niño-type warming pattern in the Pacific.

In this study, although we have presented the results from the RU simulations, we performed a parallel analysis with the RD simulations. We found the ENSO-monsoon teleconnection, which weakens during the RU period, regains its strength during the RD

simulations (Supplementary Figure S8). However, we have also found an asymmetric response of the monsoon strength under symmetric forcing during the RU and RD simulations. With this background, analysis of the reversible and irreversible components of the ENSO-monsoon teleconnection is one of our future research priorities.

It is noteworthy that, as we observed in our RU simulations, many state-of-the-art climate models indicate an El Niño-type warming in the Pacific in response to greenhouse warming[29]. However, in Cai et al.[29]'s study, CCSM4 was one of the two models which did not agree with the rest of the model simulations analyzed and exhibited a reduced El Niño variability. Although the CCSM4 in Cai et al.[29] and CESM1.2 that we have used are fundamentally similar, the simulations analyzed by Cai et al.[29] (RCP8.5 simulations) and us (see experiment details in the Methods section) are very different. Nonetheless, comparative analysis of the model's behavior under two different forcing conditions can be expected to help us not just to understand the model better but more importantly, can provide useful information relevant to the debate on the El Niño or La Niña like warming pattern in the climate models[81,82].

A recent study by Cai et al.[25] found increased pIOD events under greenhouse warming. Although they found a relationship between changes in variability or frequency of a moderate pIOD with changes in El Niño, the models exhibited an increase in El Niños but a decrease in pIOD. Therefore, Cai et al.[25] ruled out the changes in El Niño as a possible cause for this. We found conflicting results from our analysis. At this point, we do not have precise arguments to address Cai et al.[25]'s conclusion. Nonetheless, we note that Cai et al.[25]'s conclusion is based on the variability of the IOD and ENSO while our finding emphasizes the role of the mean state of the tropical oceans. Also, Cai et al.[25]'s argument seeks intermodel agreement while we have analyzed 28 ensembles of one climate model.

Our analysis of the ENSO-monsoon teleconnection rests on how the tropical oceans will interact in a warmer world. To conclude, we do not claim to settle the debate on the ENSO-monsoon teleconnection since our findings are from a climate model that may have biases[47]. Rather we intend to contribute to the debate by, based on our results, postulating that, the mean change in tropical oceans will be more important than the variability change and that will play a critical role in modulating the ENSO-monsoon teleconnection in a warmer world.

METHODS

Model configuration and experimental design

Here, we use the fully coupled Community Earth System Model version 1.2 (CESM1.2)[83]. This model is composed of the atmosphere (The Community Atmospheric Model version 5, CAM5) with a horizontal resolution of $1° \times 1°$ in longitude and latitude, respectively and 60 vertical levels[84], ocean (The Parallel Ocean Program version 2, POP2) with 60 vertical levels and a horizontal resolution of $1° \times 0.3°$ in longitude and latitude, respectively near the equator with a gradual increase to 0.5 near the pole[85], sea ice (The Community Ice Code version 4, CICE4), and land model (Community Land Model version 4, CLM4) that uses carbon-nitrogen cycle[86].

We have analyzed 28 ensembles of simulations forced by increasing atmospheric CO_2 concentration at a rate of 1% year^{-1} until CO_2 quadrupling. These simulations are part of longer simulations. For the sake of completeness, we are providing a brief description of the full length of the simulations. The model simulation starts with a present-day (PD) climate simulation for 900 years holding a constant CO_2 concentration level ($1 \times CO_2$, 367 ppm). Then 28 initial conditions were chosen from these 900 years. These initial conditions correspond to the atmospheric and oceanic states following different phases of the Pacific decadal Oscillation (PDO) and Atlantic Multidecadal Oscillation (AMO). Starting from these 28 initial conditions CO_2 varying simulations, namely, ramp-up (RU) and ramp-down (RD) simulations, were performed. Each of these RU and RD simulations is 140 years long. The RU simulations employed an increasing atmospheric CO_2 concentration at a rate of 1% year^{-1} until CO_2 quadrupling (the 1st year of RU with CO_2 concentration 1×367 ppm and the 140th year with CO_2 level 4 x 367 ppm) followed by RD simulations that employed a decreasing CO_2 at the same rate (1% year^{-1}) for 140 years until reaching a CO_2 level of 367 ppm at the end of 280th year. These scenarios PD, RU, and RD are almost the same as the carbon cycle reversibility experimental protocol (CDR-reversibility) except for the initial CO_2 level[45]. A pictorial depiction of the idealized CO_2 forcing pathways applied in our simulations is available in An et al.[44]'s Fig. 1a. Each ensemble simulation was ended with a 220 years long constant CO_2 (367 ppm) simulation, i.e., net-zero emission (restoring period).

Methodology

We have analyzed and presented the results from the 140 years of RU simulations in our study. The results presented are ensemble means unless mentioned otherwise. For the figures that depict results in 2D (latitude-longitude maps, height-latitude cross-sections, etc.) the calculations are performed for each ensemble separately first and then the mean is calculated. For the line plots, ensemble spreads have been indicated. For the indices representing ISMR, IOD, ENSO, etc, we detrended the data first to remove any long-term trend present due to constant increment in forcing. To compute the index for ISMR, rainfall anomalies are averaged over JJAS and over the region defined by the longitudes 65°E-88°E and latitudes 18°N-28°N, which indicates the approximate area of core monsoon region defined by Rajeevan et al.[87]. The dipole mode index (DMI) is used to represent the state of IOD and it is computed following the same methodology as Saji et al.[14] that is the SST anomaly difference between the western (60°E-80°E, 10°S-10°N) and eastern (90°E-110°E, 10°S-Equator) the Indian Ocean. The NINO3.4 index defined as the average JJAS SST anomalies in the Niño 3.4 region (5°N-5°S, 120°W-170°W) is used to represent the ENSO state. For calculations involving the removal of the ENSO signal from the data, we followed the same methodology as Pottapinjara et al.[66]. Essentially, all the indices are computed for the JJAS season unless otherwise mentioned.

For a preliminary analysis of the model fidelity in simulating the monsoon rainfall, we have used the India Meteorological Department (IMD) 0.25°x0.25° gridded daily rainfall data[87,88] and the Global Precipitation Climatology Project (GPCP) 2.5°x2.5° monthly product[89] as observational benchmarks. The SST observation data used in our analysis are obtained from the Hadley Centre Sea Ice and Sea Surface Temperature, version 1 (HadISST1)[90].

DATA AVAILABILITY

Data from the same model simulations as were used in Oh et al.[91] were used in the creation of this manuscript. The data are available from https://doi.org/10.6084/m9.figshare.19354055.

CODE AVAILABILITY

All codes used for analyses of the simulation data are available from the corresponding author upon reasonable request.

REFERENCES

1. Goswami, B. N. South asian summer monsoon: An overview; in the global monsoon system: Research and forecast.*Third International Workshop on Monsoon (IWM-III) (2-6 November 2004, Hangzhou, China) (TMRP 70) (WMO TD 1266)*. (2005).
2. Charney, J. G. & Shukla, J. Predictability of monsoons. *Monsoon Dynam.* 99–109 (1981).
3. Shukla, J. & Paolino, D. A. The Southern Oscillation and Long-Range Forecasting of the Summer Monsoon Rainfall over India. *Monthly Weather Rev.***111**, 1830–1837 (1983).
4. Webster, P. J. et al. Monsoons: processes, predictability, and the prospects for prediction. *J. Geophys. Res.: Oceans* **103**, 14451–14510 (1998).
5. Kumar, K. K., Rajagopalan, B. & Cane, M. A. On the weakening relationship between the Indian monsoon and ENSO. *Science* **284**, 2156–2159 (1999).
6. Annamalai, H., Hamilton, K. & Sperber, K. R. The South Asian summer monsoon and its relationship with ENSO in the IPCC AR4 simulations. *J. Clim.* **20**, 1071–1092 (2007).
7. Turner, A. G. & Annamalai, H. Climate change and the South Asian summer monsoon. *Nat. Clim.Chan.* **2**, 587–595 (2012).
8. Lee, J.-Y. & Bódai, T. Future changes of the ENSO-Indian summer monsoon teleconnection. *Ind. Summer Monsoon Variability.* 393–412 (2021).
9. Turner, A. G., Inness, P. M. & Slingo, J. M. The effect of doubled CO_2 and model basic state biases on the monsoon-enso system. I: Mean response and inter-annual variability. *Quarterly J. Royal Meteorol. Soc.* **133**, 1143–1157 (2007).
10. Azad, S. & Rajeevan, M. Possible shift in the enso-indian monsoon rainfall relationship under future global warming. *Scientific Reports.* **6** (2016).
11. Li, X. & Ting, M. Recent and future changes in the asian monsoon-enso relationship: Natural or forced? *Geophys. Res. Lett.* **42**, 3502–3512 (2015).
12. Roy, I., Tedeschi, R. G. & Collins, M. ENSO teleconnections to the Indian summer monsoon under changing climate. *Int. J. Climatol.* **39**, 3031–3042 (2019).
13. Bódai, T., Drótos, G., Herein, M., Lunkeit, F. & Lucarini, V. The forced response of the el niño-southern oscillation-indian monsoon teleconnection in ensembles of earth system models. *J. Clim.* **33**, 2163–2182 (2020).
14. Saji, N. H., Goswami, B. N., Vinayachandran, P. N. & Yamagata, T. A dipole mode in the tropical indian ocean. *Nature* **401**, 360–363 (1999).
15. Webster, P. J., Moore, A. M., Loschnigg, J. P. & Leben, R. R. Coupled ocean-atmosphere dynamics in the indian ocean during 1997-98. *Nature* **401**, 356–360 (1999).
16. Meyers, G., McIntosh, P., Pigot, L. & Pook, M. The years of el niño, la niña and interactions with the tropical indian ocean. *J. Clim.* **20**, 2872–2880 (2007).
17. Cherchi, A. & Navarra, A. Influence of ENSO and of the Indian Ocean Dipole on the Indian summer monsoon variability. *Clim. Dynam.* **41**, 81–103 (2013).
18. Ashok, K., Guan, Z. & Yamagata, T. Impact of the indian ocean dipole on the relationship between the indian monsoon rainfall and enso. *Geophys. Res. Lett.* **28**, 4499–4502 (2001).
19. Ashok, K., Guan, Z., Saji, N. H. & Yamagata, T. Individual and Combined Influences of ENSO and the Indian Ocean Dipole on the Indian Summer Monsoon. *J. Clim.* **17**, 3141–3155 (2004).
20. Ashok, K., Behera, S. K., Rao, S. A., Weng, H. & Yamagata, T. El niño modoki and its possible teleconnection. *J. Geophys. Res.: Oceans* **112** (2007).

21. Krishnaswamy, J. et al. Non-stationary and non-linear influence of enso and indian ocean dipole on the variability of indian monsoon rainfall and extreme rain events. *Clim. Dynam.* **45**, 175–184 (2015).

22. Hrudya, P. H., Varikoden, H. & Vishnu, R. A review on the Indian summer monsoon rainfall, variability and its association with ENSO and IOD. *Meteorol. Atmosph. Phys.* **33** (2021).

23. Cai, W. et al. Projected response of the indian ocean dipole to greenhouse warming. *Nat/ Geosci.* **6**, 999–1007 (2013).

24. Cai, W. et al. Increased frequency of extreme indian ocean dipole events due to greenhouse warming. *Nature* **510**, 254–258 (2014).

25. Cai, W. et al. Opposite response of strong and moderate positive indian ocean dipole to global warming. *Nat. Clim. Chan.* **11**, 27–32 (2021).

26. Ramu, D. A., Chowdary, J. S., Ramakrishna, S. S. & Kumar, O. S. Diversity in the representation of large-scale circulation associated with ENSO-Indian summer monsoon teleconnections in CMIP5 models. *Theoretical Appl. Climatol.* **132**, 465–478 (2018).

27. McKenna, S., Santoso, A., Gupta, A. S., Taschetto, A. S. & Cai, W. Indian Ocean Dipole in CMIP5 and CMIP6: characteristics, biases, and links to ENSO. *Sci. Rep.* **10** (2020).

28. Zheng, X. T., Xie, S. P., Lv, L. H. & Zhou, Z. Q. Intermodel uncertainty in ENSO amplitude change tied to Pacific Ocean warming pattern. *J. Clim.* **29**, 7265–7279 (2016).

29. Cai, W. et al. Increased variability of eastern Pacific El Niño under greenhouse warming. *Nature* **564**, 201–206 (2018).

30. Fredriksen, H. B., Berner, J., Subramanian, A. C. & Capotondi, A. How Does El Niño-Southern Oscillation Change Under Global Warming–A First Look at CMIP6. *Geophys. Res. Lett.* **47** (2020).

31. Ju, J. & Slingo, J. The asian summer monsoon and enso. *Quarterly J. Royal Meteorol. Soc* **121**, 1133–1168 (1995).

32. Lau, N.-C. & Nath, M. J. Impact of ENSO on the Variability of the Asian-Australian Monsoons as Simulated in GCM Experiments. *J. Clim.* **13**, 4287–4309 (2000).

33. Wang, B., Wu, R. & Fu, X. Pacific-East Asian Teleconnection: How Does ENSO Affect East Asian Climate? *J. Clim* **13**, 1517–1536 (2000).

34. Jang, Y. & Straus, D. M. The Indian monsoon circulation response to El Niño diabatic heating. *J. Clim.* **25**, 7487–7508 (2012).

35. Almazroui, M., Saeed, S., Saeed, F., Islam, M. N. & Ismail, M. Projections of Precipitation and Temperature over the South Asian Countries in CMIP6. *Earth Syst. Environ.* **4**, 297–320 (2020).

36. Chen, Z. et al. Global Land Monsoon Precipitation Changes in CMIP6 Projections. *Geophys. Res. Lett.* **47** (2020).

37. Ha, K. J., Moon, S., Timmermann, A. & Kim, D. Future Changes of Summer Monsoon Characteristics and Evaporative Demand Over Asia in CMIP6 Simulations. *Geophys. Res. Lett.* **47** (2020).

38. Wang, B., Jin, C. & Liu, J. Understanding Future Change of Global Monsoons Projected by CMIP6 Models. *J. Clim.* **33**, 6471–6489 (2020).

39. Katzenberger, A., Schewe, J., Pongratz, J. & Levermann, A. Robust increase of Indian monsoon rainfall and its variability under future warming in CMIP6 models. *Earth Syst. Dynam.* **12**, 367–386 (2021).

40. Zheng, X. T. et al. Indian ocean dipole response to global warming in the CMIP5 multimodel ensemble. *J. Clim.* **26**, 6067–6080 (2013).

41. Krishnamurthy, V. & Goswami, B. Indian monsoon-ENSO relationship on interdecadal timescale. *J. Clim.* **13**, 579–595 (2000).

42. Krishnamurthy, L. & Krishnamurthy, V. Influence of PDO on South Asian summer monsoon and monsoon-ENSO relation. *Clim. Dynam.* **42**, 2397–2410 (2014).

43. Yun, K. S. & Timmermann, A. Decadal monsoon-enso relationships reexamined. *Geophys. Res. Lett* **45**, 2014–2021 (2018).

44. An, S. I. et al. Global Cooling Hiatus Driven by an AMOC Overshoot in a Carbon Dioxide Removal Scenario. *Earth's Future* **9** (2021).

45. Keller, D. P. et al. The Carbon Dioxide Removal Model Intercomparison Project (CDRMIP): Rationale and experimental protocol for CMIP6. *Geosci. Model Dev.* **11**, 1133–1160 (2018).

46. Bellenger, H., Guilyardi, E., Leloup, J., Lengaigne, M. & Vialard, J. ENSO representation in climate models: From CMIP3 to CMIP5. *Clim. Dynam.* **42**, 1999–2018 (2014).

47. Meehl, G. A. et al. Monsoon regimes and processes in CCSM4. Part I: The Asian-Australian monsoon. *J. Clim.* **25**, 2583–2608 (2012).

48. Goswami, B. B. & Goswami, B. N. A road map for improving dry-bias in simulating the South Asian monsoon precipitation by climate models. *Clim. Dynam.* **49**, 2025–2034 (2017).

49. Gusain, A., Ghosh, S. & Karmakar, S. Added value of CMIP6 over CMIP5 models in simulating Indian summer monsoon rainfall. *Atmosph. Res.* **232**, 2689 (2020).

50. Choudhury, B. A., Rajesh, P. V., Zahan, Y. & Goswami, B. N. Evolution of the Indian summer monsoon rainfall simulations from CMIP3 to CMIP6 models. *Clim. Dynam.* **58**, 2637–2662 (2022).

51. Meehl, G. A. et al. Climate system response to external forcings and climate change projections in CCSM4. *J. Clim.* **25**, 3661–3683 (2012).

52. Srivastava, G., Chakraborty, A. & Nanjundiah, R. S. Multidecadal see-saw of the impact of ENSO on Indian and West African summer monsoon rainfall. *Clim. Dynam.* **52**, 6633–6649 (2019).

53. Torrence, C. & Webster, P. J. Interdecadal Changes in the ENSO-Monsoon System. *J. Clim.* **12**, 2679–2690 (1999).

54. Kumar, K. K., Rajagopalan, B., Hoerling, M., Bates, G. & Cane, M. Unraveling the mystery of Indian monsoon failure during El Niño. *Science* **314**, 115–119 (2006).

55. Ashrit, R. G., Douville, H. & Kumar, K. R. Response of the Indian monsoon and ENSO-monsoon teleconnection to enhanced greenhouse effect in the CNRM coupled model. *J. Meteorol. Soc. Japan* **81**, 779–803 (2003).

56. Ashrit, R. G., Kumar, K. R. & Kumar, K. K. ENSO-Monsoon relationship in a greenhouse warming scenario. *Geophys. Res. Lett.* **28**, 1727–1730 (2001).

57. Ashrit, R. G., Kitoh, A. & Yukimoto, S. Transient response of ENSO-monsoon teleconnection in MRI-CGCM2.2 climate change simulations. *J. Meteorol. Soc. Japan* **83**, 273–291 (2005).

58. Pillai, P. A. & Mohankumar, K. Individual and combined influence of El Niño-southern oscillation and Indian Ocean dipole on the tropospheric biennial oscillation. *Quarterly J. Royal Meteorol. Soc.* **136**, 297–304 (2010).

59. Ummenhofer, C. C., Gupta, A. S., Li, Y., Taschetto, A. S. & England, M. H. Multidecadal modulation of the El Nĩo-Indian monsoon relationship by Indian Ocean variability. *Environ. Res. Lett.* **6**, 034006 (2011).

60. Wang, X. & Wang, C. Different impacts of various El Niño events on the Indian Ocean Dipole. *Clim. Dynam.* **42**, 991–1005 (2014).

61. Terray, P., Sooraj, K. P., Masson, S. & Prodhomme, C. Anatomy of the Indian Summer Monsoon and ENSO relationships in state-of-the-art CGCMs: role of the tropical Indian Ocean. *Clim. Dynam.* **56**, 329–356 (2021).

62. Wilson, S. S. & Mohanakumar, K. Influence of subtropical circulation systems on the changing El Niño-Indian summer monsoon relationship. *Atmos. Res.* **252**, 105457 (2021).

63. Sabeerali, C. T., Ajayamohan, R. S., Bangalath, H. K. & Chen, N. Atlantic zonal mode: An emerging source of indian summer monsoon variability in a warming world. *Geophys. Res. Lett.* **46**, 4460–4467 (2019).

64. Kucharski, F., Bracco, A., Yoo, J. H. & Molteni, F. Atlantic forced component of the Indian monsoon interannual variability. *Geophys. Res. Lett.* **35**, GL033037 (2008).

65. Chang, P., Fang, Y., Saravanan, R., Ji, L. & Seidel, H. The cause of the fragile relationship between the Pacific El Nĩo and the Atlantic Nĩno. *Nature* **443**, 324–328 (2006).

66. Pottapinjara, V., Girishkuma, M. S., Ravichandran, M. & Murtugudde, R. Influence of the atlantic zonal mode on monsoon depressions in the Bay of Bengal during boreal summer. *J. Geophys. Res.* **119**, 6456–6469 (2014).

67. Pottapinjara, V., Girishkumar, M. S., Sivareddy, S., Ravichandran, M. & Murtugudde, R. Relation between the upper ocean heat content in the equatorial Atlantic during boreal spring and the Indian monsoon rainfall during June-September. *Int. J. Climatol.* **36**, 2469–2480 (2016).

68. Pottapinjara, V. et al. Simulation of interannual relationship between the Atlantic zonal mode and Indian summer monsoon in CFSv2. *Clim. Dynam.* **57**, 353–373 (2021).

69. Roxy, M. K. et al. Twofold expansion of the Indo-Pacific warm pool warps the MJO life cycle. *Nature* **575**, 647–651 (2019).

70. An, S.-I. et al. Intensity changes of Indian Ocean dipole mode in a carbon dioxide removal scenario. *npj Clim. Atmos. Sci.* **5**, 20 (2022).

71. Cai, W. et al. Enso and greenhouse warming. *Nat. Clim. Chan.* **5**, 849–859 (2015).

72. Ratna, S. B., Cherchi, A., Osborn, T. J., Joshi, M. & Uppara, U. The extreme positive indian ocean dipole of 2019 and associated indian summer monsoon rainfall response. *Geophys. Res. Lett.* **48**, e2020GL091497 (2021).

73. Stuecker, M. F. et al. Revisiting ENSO/Indian Ocean Dipole phase relationships. *Geophys. Res. Lett.* **44**, 2481–2492 (2017).

74. Polonsky, A. & Torbinsky, A. The iod-enso interaction: The role of the indian ocean current's system. *Atmosphere.* **12**, 1662 (2021).

75. Annamalai, H., Xie, S. P., McCreary, J. P. & Murtugudde, R. Impact of Indian Ocean Sea surface temperature on developing El Niño. *Journal of Climate* **18**, 302–320 (2005).

76. Izumo, T. et al. Influence of the state of the indian ocean dipole on the following years el nĩo. *Nat. Geosci.* **3**, 168–172 (2010).

77. An, S.-I. A dynamic link between the basin-scale and zonal modes in the tropical Indian Ocean. *Theor. Appl. Climatol.* **78**, 203–215 (2004).

78. Guo, F., Liu, Q., Sun, S. & Yang, J. Three types of Indian Ocean dipoles. *J. Clim.* **28**, 3073–3092 (2015).

79. Zhao, Y. & Nigam, S. The Indian ocean dipole: A monopole in SST. *J. Clim.* **28**, 3–19 (2015).

80. Chakraborty, A. & Singhai, P. Asymmetric response of the Indian summer monsoon to positive and negative phases of major tropical climate patterns. *Sci. Rep.* **11**, 22561 (2021).

81. Lian, T., Chen, D., Ying, J., Huang, P. & Tang, Y. Tropical Pacific trends under global warming: El Niño-like or La Niña-like? *Natl. Sci. Rev.* **5**, 810–812 (2018).

82. Luo, J. J., Wang, G. & Dommenget, D. May common model biases reduce CMIP5's ability to simulate the recent Pacific La Niña-like cooling? *Clim. Dynamics* **50**, 1335–1351 (2018).

83. Hurrell, J. W. et al. The community earth system model: A framework for collaborative research. *Bull. Am. Meteorol. Soc.* **94**, 1339–1360 (2013).

84. Neale, R. B. et al. Description of the NCAR Community Atmosphere Model (CAM 5.0). *National Center for Atmospheric Research Technical Note* NCAR/TN–486+STR (2010).

85. Smith, R. et al. The parallel ocean program (POP) reference manual ocean component of the community climate system model (CCSM) and community earth system model (CESM). *LAUR-01853* **141**, 1–140 (2010).

86. Lawrence, D. M. et al. Parameterization improvements and functional and structural advances in Version 4 of the Community Land Model. *J. Adv. Model. Earth Syst.* **3**, MS00045 (2011).

87. Rajeevan, M., Gadgil, S. & Bhate, J. Active and break spells of the indian summer monsoon. *J. Earth Syst. Sci.* **119**, 229–247 (2010).

88. Pai, D. S., Sridhar, L., Badwaik, M. R. & Rajeevan, M. Analysis of the daily rainfall events over india using a new long period (1901-2010) high resolution (0.25° × 0.25°) gridded rainfall data set. *Clim. Dynamics* **45**, 755–776 (2015).

89. Adler, R. F. et al. The version-2 global precipitation climatology project (GPCP) monthly precipitation analysis (1979–present). *J. hydrometeorol.* **4**, 1147–1167 (2003).

90. Rayner, N. A. et al. Global analyses of sea surface temperature, sea ice, and night marine air temperature since the late nineteenth century. *J. Geophys. Res.: Atmosph.* **108**, D002670 (2003).

91. Oh, J.-H., An, S.-I., Shin, J. & Kug, J.-S. Centennial memory of the Arctic Ocean for future Arctic climate recovery in response to a carbon dioxide removal. *Earth's Future* **10**, e2022EF002804 (2022).

AUTHOR CONTRIBUTIONS

B.B.G. performed the analyses in discussion with S-I.A. All authors interpreted and discussed the results. B.B.G. drafted the manuscript with S-I.A. contributing to its content. All authors approved the final manuscript.

COMPETING INTERESTS

The authors declare no competing interests.

ADDITIONAL INFORMATION

Supplementary information The online version contains supplementary material available at https://doi.org/10.1038/s41612-023-00411-5.

Correspondence and requests for materials should be addressed to Soon-Il An.

Reprints and permission information is available at http://www.nature.com/reprints

Publisher's note Springer Nature remains neutral with regard to jurisdictional claims in published maps and institutional affiliations.